The Solvation Structure of Fulleride C_{60}^{5-} Anions in Potassium Ammonia Solution

Christopher A. Howard,* Jonathan C. Wasse, and Neal T. Skipper

London Centre for Nanotechnology, Department of Physics and Astronomy, University College London, Gower Street, London, WC1E 6BT, UK

Helen Thompson and Alan K. Soper

ISIS Facility, Rutherford Appleton Laboratory, Chilton, Oxfordshire, OX11 0QX, UK

Received: October 13, 2006; In Final Form: January 29, 2007

The solvation of the fulleride anion C_{60}^{5-} has been studied in concentrated potassium-ammonia solution using advanced neutron diffraction techniques. Isotopic substitution of hydrogen for deuterium in conjunction with second-order difference analysis has allowed us to obtain a detailed picture of the solvent structure. Because of the complexity of our system, we have visualized this structure via empirical potential structural refinement. This method provides us with a full three-dimensional molecular model of our system that is consistent with the experimental data. The results reveal the way in which hydrogen bonds between the solvent and solute assemble to accommodate high concentrations of monodisperse fulleride anions in solution. We find that each C_{60}^{5-} has two distinct solvation shells containing ∼45 and ∼80 ammonia molecules at distances of ∼6.6 and ∼9.5 Å, respectively. This solvation effectively doubles the fulleride radius to ∼10.5 Å. Within the first solvation shell, each ammonia molecule forms an average of around one hydrogen bond to the fulleride anion, thereby allowing for intersolvent hydrogen bonding to be maintained. We find that the potassium cations are solvated by approximately six ammonia molecules at an average distance of around 2.87 Å. This is consistent with the solvation observed in bulk metal-ammonia solutions. This work therefore highlights the mechanisms by which metal-ammonia solutions are able to dissolve high concentrations of fullerenes.

1. Introduction

Since its discovery in 1985,[1] Buckminsterfullerene (C_{60}) has been the subject of intensive scientific and technological activity.[2,3] Many of the greatest challenges of fullerene science are posed by the low solubility of these molecules in most common solvents.[4] This limits our ability to manipulate fullerenes and their derivatives and restricts their characterization by solution techniques. Indeed, a major breakthrough of experimental fullerene science was the discovery by Krätschmer et al.[5] that C_{60} is soluble in benzene to about 1.5 mg/mL.[4] This allowed workable quantities of C_{60} (fullerite) crystal to be precipitated from solution. However, in aromatic liquids such as benzene the interaction energy of the fullerene with the solvent is of the same order as the interaction energy between fullerene molecules in the crystal solid.[4] As a result, the C_{60} molecules tend to form fractal aggregates in solution.

Uncharged fullerenes are almost insoluble in polar solvents.[4] Nevertheless, an important route to fulleride dissolution involves metal-ammonia solutions.[6] These liquids contain solvated electrons, which allow us to exploit the redox chemistry of fullerene in solution via sequential reduction of C_{60} fullerite crystals to soluble C_{60}^{n-} anions ($n = 1$ to 5).[7−9] In addition to providing a unique arena in which to study fulleride anions, concentrated fulleride-metal-ammonia solutions are showing great promise for purification, charge storage, and thin film deposition. Further interest stems from the fact that (reversible) removal of the ammonia produces fulleride salts, including the A_3C_{60} superconductors.[6] The T_c of these compounds increases linearly with increasing lattice parameter and can reach up to 40 K.[2] It has also been shown that the superconducting transition temperature of the compound Na_2CsC_{60} can be increased from 10.5 to 29.6 K upon ammoniation, whereby ammonia molecules solvate the sodium ions and thereby increase the lattice parameter from 14.132 to 14.473 Å.[10] However, in the case of the system $(NH_3)_xNaA_2C_{60}$ ($0.5 < x < 1$, A = K, Rb) the T_c increases with decreasing ammonia content.[11] Structural studies via powder diffraction have shown that the ammonia molecules coordinate to the metal ions within the salts, resulting in an off-centering of the Na^+ cation. The ammonia molecules themselves, as well as coordinating to the cation, form close hydrogen bonds to the C_{60}^{3-} anions (N···C ∼ 2.5 Å).[12] In contrast to this rather detailed understanding of the crystalline salts, little is known about the structure of the parent metal-ammonia-fulleride solutions. Key questions center on the mechanisms of fulleride dissolution and the potentially subtle interplay between hydrogen bonding, cation and fulleride solvation, and cation−fulleride pairing. It is also to be established whether monodisperse or aggregated fulleride species predominate.

Neutron diffraction has recently unraveled many of the structural properties of metal-ammonia solutions. In particular, isotopic substitution of hydrogen (H) for deuterium (D) has been applied to the solvent structure and has revealed the nature and extent of H-bonding and the fundamental mechanisms of cation and electron solvation.[13] In this context, the use of three-dimensional (3D) modeling via the so-called empirical potential structure refinement (EPSR)[14−16] has proved invaluable. This method produces an ensemble molecular model of the system

* Corresponding author. Email: c.howard@ucl.ac.uk.

10.1021/jp066743+ CCC: $37.00
Published on Web 04/12/2007

and allows one to extract all of the spatial distributions of the molecules, including their relative orientations. Such an approach is essential if we are to interpret data from a system as complex as a metal-ammonia-fulleride solution. In this paper, we address these questions via liquid-state neutron diffraction, following our preliminary communication,[17] to provide a complete structural picture of these solutions.

2. Theory

The quantity measured in a neutron-scattering experiment is the differential cross-section. After appropriate corrections, this will yield the total structure factor, $F(Q)$. This is a weighted sum of the different partial structure factors, arising from the correlations between different pairs of atoms

$$F(Q) = \sum_{\alpha}\sum_{\beta} c_\alpha c_\beta \bar{b}_\alpha \bar{b}_\beta [S_{\alpha\beta}(Q) - 1] \quad (1)$$

where c_α is the atomic fraction of species α, b_α is the neutron-scattering length of atom α, $Q = 4\pi\,(\sin\theta)/\lambda$ (i.e., the magnitude of the momentum change vector of the scattered neutrons), and $S_{\alpha\beta}(Q)$ is the Faber−Ziman partial structure factor involving atoms α and β only. The partial structure factor, $S_{\alpha\beta}(Q)$, contains information about correlations between the two atomic species α and β in Q-space and is defined as

$$S_{\alpha\beta}(Q) - 1 = \frac{4\pi\rho_0}{Q}\int_0^\infty r[g_{\alpha\beta}(r) - 1]\sin(Qr)\,\mathrm{d}r \quad (2)$$

where ρ_0 is the atomic number density of the sample and $g_{\alpha\beta}(r)$ is the partial distribution function for the relative density of atoms of type β as a function of their distance, r, from one of type α.

In many cases, neutrons scatter differently from different isotopes of the same atomic species. This means that isotope substitution can be used to measure only the correlations from the substituted atoms. This technique is most appropriate for isotopes with a large difference in their scattering lengths, such as D ($b_D = 6.67$ fm) and H ($b_H = -3.74$ fm). If we now refer to the substituted protons as H and all other atoms as X, then there are three composite partial structure factors (CPSFs): $S_{HH}(Q)$, $S_{XH}(Q)$, and $S_{XX}(Q)$. A first-order difference between two isotopically distinct samples will contain only $S_{HH}(Q)$ and $S_{XH}(Q)$, while a second-order difference between three isotopically distinct samples will contain only $S_{HH}(Q)$.

In the case of second-order H/D isotopic substitution, the $F(Q)$ can be written formally as the sum of the three composite partial structure factors

$$F(Q) = c_X^2 b_X^2 [S_{XX}(Q) - 1] + 2c_X c_H b_X b_H^2 [S_{XH}(Q) - 1] + c_H^2 b_H^2 [S_{HH}(Q) - 1] \quad (3)$$

where the composite coherent-scattering length, b_X, and concentration, c_X, are defined by

$$b_X = \sum_{\alpha\neq\beta} \frac{c_\alpha b_\alpha}{c_X} \text{ and } c_X = \sum_{\alpha\neq\beta} c_\alpha \quad (4)$$

Because $c_H = (1 - c_X)$, the $S_{HH}(Q)$ composite structure factor can then be calculated as the following:

$$S_{HH}(Q) = \frac{xF_H(Q) + (1-x)F_D(Q) - F_{HD}(Q)}{c_H^2[xb_H^2 + (1-x)b_D^2 - b_{HD}^2]} \quad (5)$$

where subscripts H and D refer to the hydrogenated and deuterated samples, respectively, and HD as a mixture sample with x being the fraction of the light sample in this mixture. Therefore

$$b_{HD} = xb_H + (1-x)b_D \quad (6)$$

Similarly, the $S_{XH}(Q)$ and $S_{XX}(Q)$ partial structure factors are calculated from the following equations:

$$S_{XH}(Q) - 1 = \frac{F_H(Q) - F_D(Q) - c_H^2(b_D^2 - b_H^2)[S_{HH}(Q) - 1]}{2c_X c_H b_X (b_H - b_D)}$$

$$S_{XX}(Q) - 1 = \frac{F_H(Q) - 2c_H c_X b_H b_X [S_{XH}(Q) - 1] - c_H^2 b_H^2 [S_{HH}(Q) - 1]}{c_X^2 b_X^2} \quad (7)$$

The weighting factors for the partial terms contributing to the composite partial structure factors are

$$S_{XH}(Q) - 1 = \frac{\sum_{\alpha\neq H} c_\alpha b_\alpha [S_{\alpha H}(Q) - 1]}{c_X b_X} \quad (8)$$

$$S_{XX}(Q) - 1 = \frac{\sum_{\alpha\neq H,\beta\neq H} c_\alpha b_\alpha c_\beta b_\beta [S_{\alpha\beta}(Q) - 1]}{c_X^2 b_X^2} \quad (9)$$

3. Experimental Methods

We have studied a solution of composition $C_{60}K_5(NH_3)_{250}$ (see Figure 1). This ratio of potassium to C_{60} ensures a maximum charging of the fullerene to C_{60}^{5-}, which intuitively yields the most highly developed solvent structure. Three isotopically distinct samples were measured: (1) $C_{60}K_5(NH_3)_{250}$, (2) $C_{60}K_5(ND_3)_{250}$, and a 50:50 mixture of (1) and (2). This approach permits the extraction of the three composite partial structure factors $S_{HH}(Q)$, $S_{XH}(Q)$, and $S_{XX}(Q)$. The relative weightings of the individual partial structure factors in these composites depend on the relative concentration and neutron-scattering power of the individual atomic species involved and are shown in Table 1; only one correlation (H−H) contributes to $S_{HH}(Q)$. As can be seen, the C−N and C−H correlations are strongly weighted in the data.

Diffraction data were collected at the small angle neutron diffractometer for liquids and amorphous samples (SANDALS) at the ISIS spallation neutron source at the Rutherford Appleton Laboratory, U.K. SANDALS is optimized for the measurement of the structure of liquid and amorphous samples and in particular for H/D substitution.[18]

The solutions were prepared in situ by condensing a known amount of anhydrous ammonia gas onto preweighed potassium metal and C_{60} fullerite powder under vacuum conditions at 230 K. The dissolution takes approximately 2 h.[6] The fullerene powder and potassium metal were loaded in a dry argon glovebox (O_2 and H_2O < 2 ppm) in a flat-plate null coherent-scattering titanium/zirconium cell with 1 mm sample and wall thicknesses. This geometry minimizes multiple neutron-scattering and absorption corrections. The temperature was maintained via a closed-cycle refrigerator on the beam line. Prior to the in situ condensation of ammonia, the cell was connected to a purpose-built stainless steel gas rig via a 1/8" capillary and was evacuated to a pressure of less than 10^{-5} mbar. This method

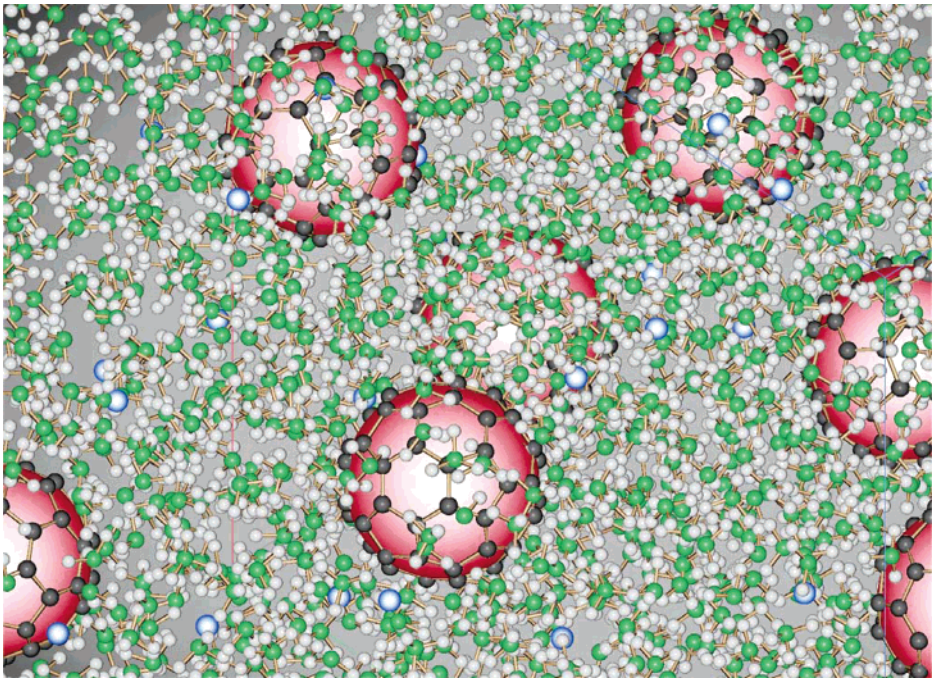

Figure 1. Molecular graphics snapshot of the system $K_5C_{60}(NH_3)_{250}$ taken from the EPSR ensemble fit to the diffraction data. Key: fulleride, red; carbon, black; potassium ion, blue; hydrogen, white; nitrogen, green.

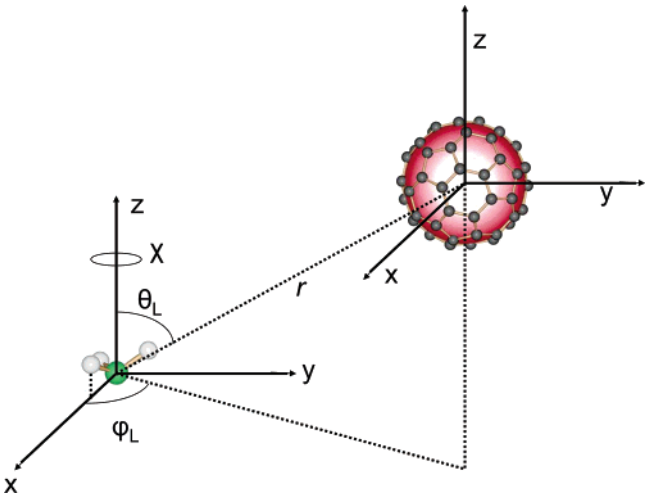

Figure 2. The coordinate system used to investigate the 3D spatial density distributions of the system. The figure shows how the orientation of the ammonia molecule at the origin is fixed.

TABLE 1: Relative Interatomic Neutron-Scattering Weights for $C_{60}K_5(NH_3)_{250}$ (eqs 8 and 9)

X−X correlation	coefficient	X−H correlation	coefficient
N−N	0.7203	N−H	0.8487
N−K	0.0113	K−H	0.0067
N−C	0.2455	C−H	0.1446
C−C	0.0209		
K−C	0.0019		
K−K	4.43×10^{-5}		

has been successfully used on the same instrument for previous studies on metal-ammonia solutions.[13,19] Typical counting times were ~10 h for each of the three samples. Before merging the individual (detector averaged) 2 h long data runs, the runs themselves were investigated as a function of time, to ensure the C_{60} was not still dissolving. For data correction and calibration, scattering data were also collected from the empty instrument (with and without the empty sample cell), and an incoherent-scattering vanadium standard slab of thickness

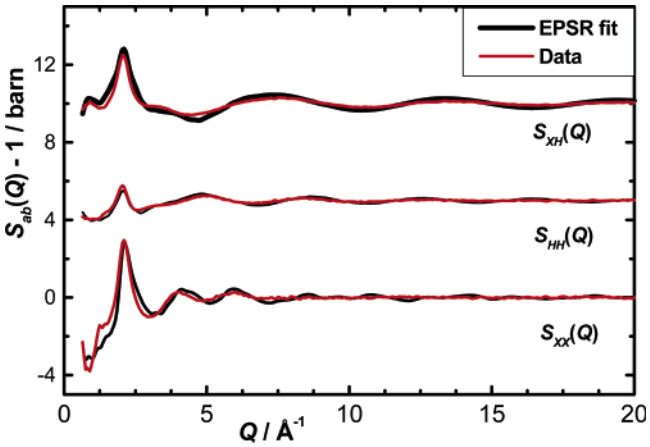

Figure 3. EPSR fits (red) to the measured CPSFs (black, eqs 5−9) obtained from the second-order difference for the solution composition $K_5C_{60}(NH_3)_{250}$.

3.48(2) mm. Background, multiple scattering, absorption, and normalization correction procedures were implemented by the ATLAS suite of programs,[20] to give the differential-scattering cross-section for each isotopically distinct sample. Polynomials representing the self-scattering and inelastic-scattering were then subtracted from the normalized differential cross-sections to yield the total static structure factors. The three target CPSFs, $S_{HH}(Q)$, $S_{XH}(Q)$, and $S_{XX}(Q)$, were formed using eqs 3−9. A minimum noise transform was used to produce the radial distribution functions presented here in Figure 3. This method of Fourier transformation is an iterative technique that attempts to generate pair correlation functions, $g_{R\hat{a}}(r)$, which are as smooth as possible while still consistent with the data.[21] In this way, we are able to focus on real features and not those that might be caused by truncation of the structure factor and/or noise within the data for example. The efficacy of these procedures was verified by checking the self-consistency of the CPSFs and their Fourier back-transforms.

4. EPSR Analysis

The technique of EPSR[14,15] aims to maximize the information that can be extracted from a set of diffraction experiments on a disordered system. This method produces a 3D ensemble of particles that is consistent with the measured diffraction data. The technique effectively uses the diffraction data as a constraint against which to refine a classical molecular simulation of the system under study.

The detailed theory behind the EPSR technique is discussed elsewhere.[14,15] In brief, the method starts with an equilibrated Monte Carlo simulation based on initial "seed" potentials. The procedure then iteratively modifies these potentials until they recreate the diffraction data. The technique allows known prior information, such as molecular geometry, overlap, and electrostatic constraints, to be built into the refinement procedure.[22]

EPSR simulations were carried out on the data using the composite partial structure factors, $S_{HH}(Q)$, $S_{XH}(Q)$, and $S_{XX}(Q)$ for the refinement. The EPSR ensemble consists of a cubic box of side ~42.6 Å containing 2000 ammonia molecules, 8 C_{60}^{5-} anions, and 40 potassium cations. The seed potentials are classical Lennard-Jones pairwise and effective charge Coulomb. The seed ammonia molecule is the 4-site OPLS model,[23,24] which has been used in a similar study on lithium-ammonia solutions.[13] The potassium potentials are taken from ref 25. The seed Lennard-Jones C_{60} carbon potentials were taken from an early atomistic classical simulation of fullerite crystal.[26] The charge on the fulleride was evenly distributed across the fixed carbon atoms (i.e., −5/60 e on each carbon atom). A reference "dummy" site was included at the center of mass of the C_{60}^{5-} to allow calculation of the respective distribution functions.

The molecular distributions resulting from the EPSR atomic configurations were visualized via a spherical harmonic expansion for the molecular pair correlation functions. This approach allows us to show the orientational correlations between molecules in the form of spatial density plots. These are obtained by holding molecule 1 fixed at the origin in a predefined orientation and then ascertaining the most probable angular coordinates of a second molecule as a function of specified distances. In this work, the molecule fixed at the origin is ammonia (see Figure 2). The angles θ and ϕ are respectively defined relative to the *z*-axis (dipole moment) and the *x*-*z* plane (in which the first intramolecular N−H bond lies) of the ammonia molecule.

5. Results and Discussion

The total-normalized structure factors for the three samples, $C_{60}K_5(NH_3)_{250}$, $C_{60}K_5(ND_3)_{250}$, and $C_{60}K_5(ND_3/NH_3)_{125:125}$ are shown in Figure 3 together with the EPSR fits. The *Q*-range measured was from 0.5 to 50 $Å^{-1}$, but the data are only plotted to 20 $Å^{-1}$ to allow us to see the salient features more clearly. The density used throughout the analysis of this experiment was 0.9 g/cm^3. This value was estimated from absorption measurements via the incident and transmission monitors on SANDALS and was checked via computer simulation. Further consistency checks were performed by back-transformation of the real space functions and then comparing with the original data.

The real space data, shown in Figure 4, reveal the expected intramolecular correlations from the fulleride, visible in the $g_{XX}(r)$ at ~1.4 Å (these are the most abundant and therefore strongly weighted shorter bond lengths in the C_{60} anion). This is the first time C_{60} has been detected directly in solution by diffraction. Likewise, the intramolecular structure of the ammonia solvent molecules can be seen at ~1.6 and ~1 Å, in the $g_{HH}(r)$ and $g_{XH}(r)$, respectively. There is no evidence here of a distortion of the ammonia molecule from the structure found in pure liquid ammonia.[27]

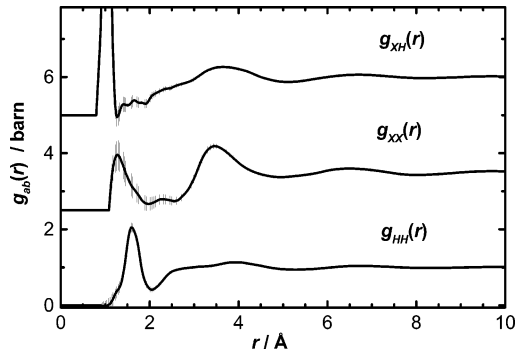

Figure 4. The real space partial distribution functions $g_{HH}(r)$, $g_{XH}(r)$, and $g_{XX}(r)$.

Upon inspection, the CPSFs show some interesting intermediate range features, such as a small prepeak before the principal peak at ~0.9 $Å^{-1}$ in the $S_{XH}(Q)$ and a shoulder on the principle peak at ~1.1 $Å^{-1}$ in the $S_{XX}(Q)$. These features correspond to correlations in real space at $\sim 2\pi/Q$, giving distances of ~7 Å and ~6 Å from the $S_{XH}(Q)$ and $S_{XX}(Q)$ functions, respectively. These distances can be explained by the existence of a well-ordered second solvation shell around the C_{60} with the nitrogen atoms being closer on average to the carbon than the hydrogen atoms. Note, however, that the feature in $S_{XX}(Q)$ can be partly explained by cross-fulleride carbon−carbon correlations. Indeed, unambiguous interpretation of individual intermediate range features is difficult.[28]

The first solvation shell will then occur at distances of approximately 2−5 Å from the carbons atoms on the fulleride. However, C−N correlations in this range would fall within the large principal peak, which arises from the more abundant nearest-neighbor intersolvent N−N correlations. To make further progress in these intermediate and short-range regimes, we must turn to our EPSR model fitting.

The EPSR fits closely mimic the experimental data, but there are some subtle differences (Figure 3). These are found mainly at low-*Q* in the $S_{XX}(Q)$ in particular and can be explained by an imperfect removal of inelastic-scattering.[29] Otherwise, all the salient features in the data are very well reproduced. Care must be taken to ensure that the simulation is actually accessing all areas of phase space and that the resulting physical model is realistic. Tests on the technique so far indicate that refining the initial seed potentials to recreate the diffraction data yields ensembles that recreate the topology of the local order.[15] From our model we are then able to calculate all 10 partial pair distribution functions for our system (eq 2), as shown in Figure 5. Where there is a distinct peak indicating a specific organization of one atom around another (usually limited to nearest-neighbors in liquids), coordination numbers have been recorded in Table 2. These numbers were determined by counting pairs at every EPSR iteration over a specific distance range $r_{min} < r < r_{max}$ spanning minima in the respective $g_{\alpha\beta}(r)$. The coordination numbers are then averaged over a number of iterations, and their errors correspond to the root mean square (rms) deviation. The better defined a feature (i.e., sharper the peak), the smaller the percentage error on the coordination number. The neutron weightings recorded in Table 1 must also be considered while examining the individual partials; the lower the weighting, the more EPSR becomes weighted more toward the simulation than the data.

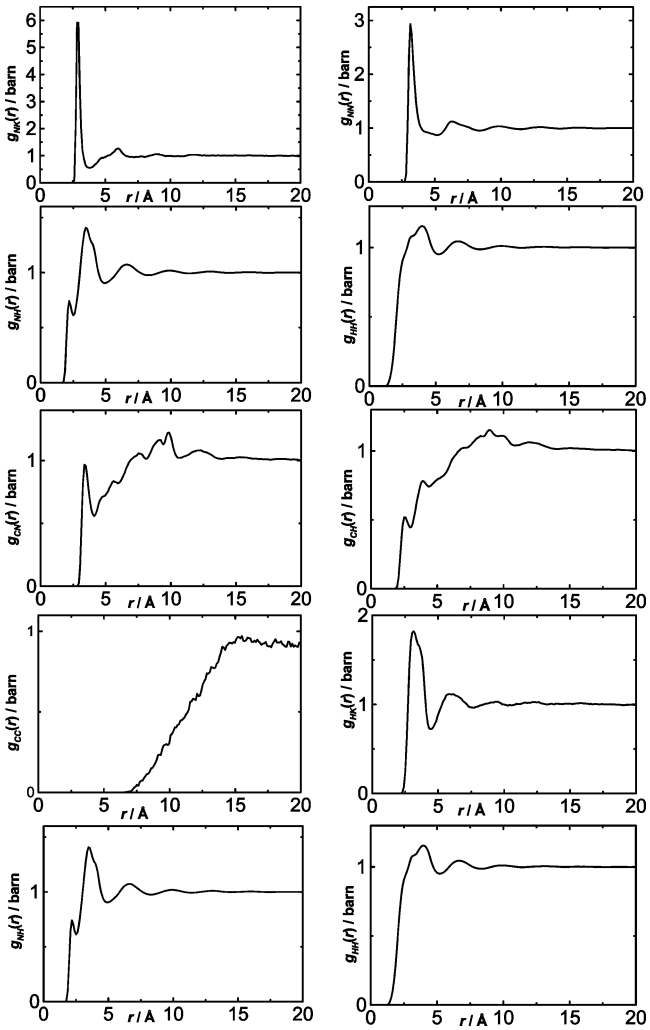

Figure 5. The individual site−site radial distribution factors, $g_{\alpha\beta}(r)$, for the 10 pairs of atom types in the solution.

TABLE 2: Coordination Numbers Obtained from the $g_{\alpha\beta}(r)$ Values Shown in Figure 5 with Integration between the Limits r_{min} and r_{max}

correlation	r_{min} (Å)	r_{max} (Å)	coordination number
N−N	2.6	5.2	14.4 ± 1.5
N−H	1.8	2.5	1.7 ± 0.9
C−N	2.9	4.1	3.2 ± 0.8
C−H	1.9	2.9	2.3 ± 0.8
C−H	2.9	4.4	13.2 ± 2.3
C−K	2.6	3.9	0.1 ± 0.3
K−N	2.5	3.6	6.6 ± 1.1
K−H	2.2	4.5	30.1 ± 3.5

5.1. Solvent−Solvent Structure. We begin our detailed discussion of the EPSR model ensemble with the intersolvent structure of the solutions (i.e., the effect of the fulleride on the bulk ammonia matrix). This is investigated by examining the pair distribution functions $g_{HH}(r)$, $g_{NH}(r)$, $g_{NN}(r)$ (Figure 5).

The $g_{HH}(r)$ function is very similar to that measured for pure ammonia[27] and has two broad peaks at ∼2.9 and 3.9 Å. The correlation, which is visible at 2.9 Å, is equivalent to the distance between two adjacent hydrogen-bonded molecules.[27] Most intersolvent H-bonding information can then be found in the $g_{NH}(r)$, with nearest-neighbor interactions manifesting themselves as a prepeak at a distance of ∼2.2 Å. This distance is lower than the corresponding feature in pure ammonia,[27] and the peak itself is more prominent in the fulleride solution. The shorter N···H hydrogen bond is a result of a tightening of the solvent structure in accommodating the fulleride.

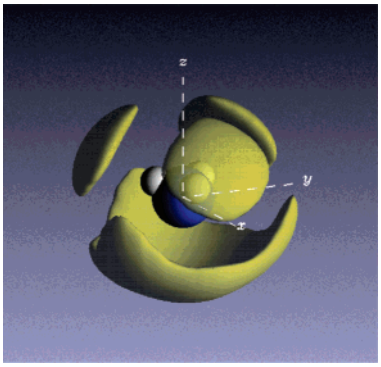

Figure 6. 3D average structure of H-bonding between ammonia molecules in the solution $K_5C_{60}(NH_3)_{250}$. The yellow region shows the most likely angular positions that an ammonia molecule in any orientation can be found in with respect to a fixed ammonia molecule (see Figure 2). This figure plots the 20% most likely positions for ammonia−ammonia distances in the range 0−5.2 Å.

The average H-bond distance in liquid ammonia has been reported to be 2.25[30] and 2.42 Å[27] in recent neutron isotopic substitution measurements. Both of these experiments report the number of H-bonds as ∼2 per nitrogen atom. The discrepancy in hydrogen-bond length may be attributed to a difference in temperature between the two measurements, but is more likely to be due to the broad nature of the shoulder and hence the inexact definition of the bond length. In the case of the fulleride solution, this H-bond shoulder resolves itself into a quite clear peak. If we examine the average number of H-bonds per nitrogen in this case, we obtain the result of ∼1.7 ± 0.9, which is lower than in bulk ammonia. The broader feature seen at about 3.6 Å is due to nonhydrogen-bonded van der Waals contacts and is similar to that found in pure ammonia.

The N−N function contains a principal peak at ∼3.18 Å, which compares to a larger distance of about ∼3.46 Å found in pure ammonia.[27] This shift is indicative of an increase in density in the fulleride solution and can be attributed to a tighter binding between ammonia molecules in the solvent due to the accommodation of the fullerides consistent with the N−H structure. Integration out to 5.2 Å yields a N−N coordination number of ∼14 for the current fulleride solution, which is the same as the value found for pure ammonia.

The 3D ammonia−ammonia average structure is shown in Figure 6. This density distribution is calculated by holding an ammonia molecule in a fixed reference orientation (Figure 3) and then calculating the top 20% of most likely positions for the approach of another ammonia molecule. This quantity is averaged over the entire system for molecule−molecule distances within the nearest-neighbor first shell (i.e., up to separations of 5.2 Å). The direction of the H-bonding can be seen clearly from the acceptor lobes, which are found above the hydrogen atoms in the ammonia at the origin. This is very similar to the structure developed in dilute metal-ammonia solutions (i.e., the metal concentration used here).[27] However, in our current solutions the number of H-bonds per nitrogen atom is slightly reduced with respect to the bulk, due to the coordination of the solvent to the large anionic species.

5.2. Fulleride Solvation Structure. The $g_{CN}(r)$ shown in Figure 5 has a peak at 3.3 Å, and the $g_{CH}(r)$ function has peaks at 2.6 and 2.9 Å. These features are attributed to an intense ordering of the solvent around the fulleride. For more insight, the two-dimensional (2D) spatial density distribution of ammonias around a C_{60}^{5-} center of mass is shown in Figure 7.

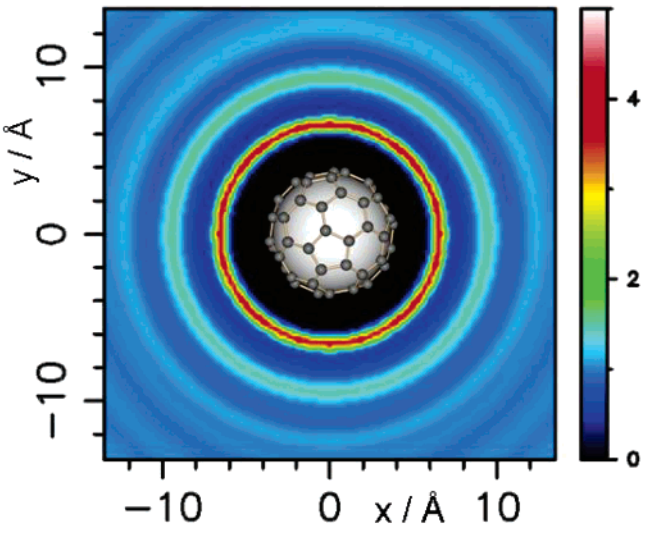

Figure 7. 2D projection of the $NH_3-C_{60}^{5-}$ solvent structure in the solution. This figure shows the ensemble average relative density of ammonia molecules around a reference fulleride located at the origin.[32]

TABLE 3: Coordination Numbers Obtained from the $g_{\alpha\beta}(r)$ Values Shown in Figures 8 and 11 with Integration between the Limits r_{min} and r_{max}[a]

correlation	r_{min} (Å)	r_{max} (Å)	coordination number
$C_{60}-N$	0	7.5	44.6 ± 1.9
$C_{60}-N$	8	10.5	79.6 ± 3.5
$C_{60}-H$	0	6.2	39.7 ± 2.2
$C_{60}-H$	6.2	7.6	96.2 ± 4.6

[a] C_{60} represents the fulleride center of mass.

The relevant coordination numbers for the solvation shells are presented in Table 3. These data immediately reveal a dense spherical first solvation shell of ammonia at a distance of 5.5−7.5 Å from the center of the C_{60}^{5-} anion (cage diameter 3.54 Å). Beyond this, the second solvation shell is at a distance of 8−10.5 Å with the anion's influence on the solvent matrix still discernible at larger distances. This is in agreement with the initial conclusions drawn on the data before EPSR analysis. The average fulleride-nitrogen coordination numbers within the first and second solvation shells are ∼45 and 80 ammonias, respectively. The intensity of these shells is large, and the question now is how are the solvent molecules oriented in these shells?

To focus on the fulleride solvation, the $g_{\alpha\beta}(r)$ values for the distribution of nitrogen and hydrogen atoms around the center of mass of the C_{60}^{5-} anion are plotted in Figure 8. Visual inspection of these functions shows clearly the preferred orientation of the ammonia molecules in the first solvation shell. The relative intensities of the first two peaks (at ∼5.5 and 7.1 Å; see Table 3) confirm that the molecules in this first shell adopt a position with (on average) one hydrogen atom pointing toward the center of the C_{60}^{5-} anion.

A 3D representation of this H-bonding is shown in Figure 9. This was obtained by holding the ammonia molecule in a fixed orientation, and plotting the average distribution of C_{60}^{5-} (center of mass). The figure plots the isosurfaces of the top 50 and 90% of the most likely angular positions of a C_{60}^{5-} around a fixed ammonia molecule for distances equivalent to the two solvation shells. The results confirm that within the first solvation shell the ammonia molecules are aligned with one hydrogen atom pointing toward the center of the fulleride anion. In the second shell, it can be seen that although this directionality is still present, it is weaker and includes molecules in which

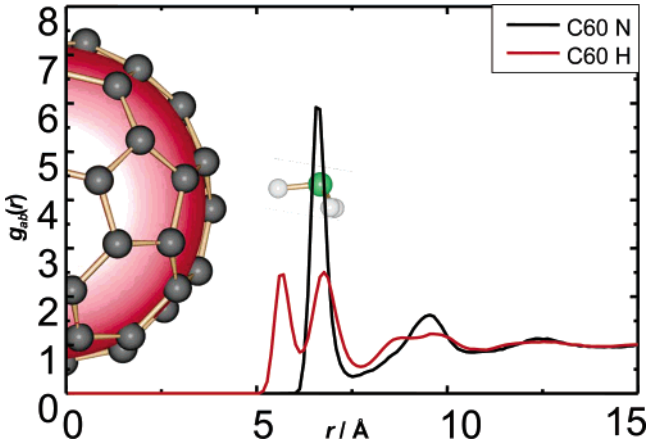

Figure 8. Pair distribution functions $g_{\alpha\beta}(r)$ of nitrogen and hydrogen around the center of mass of a fulleride anion with molecular graphics to guide the eye.

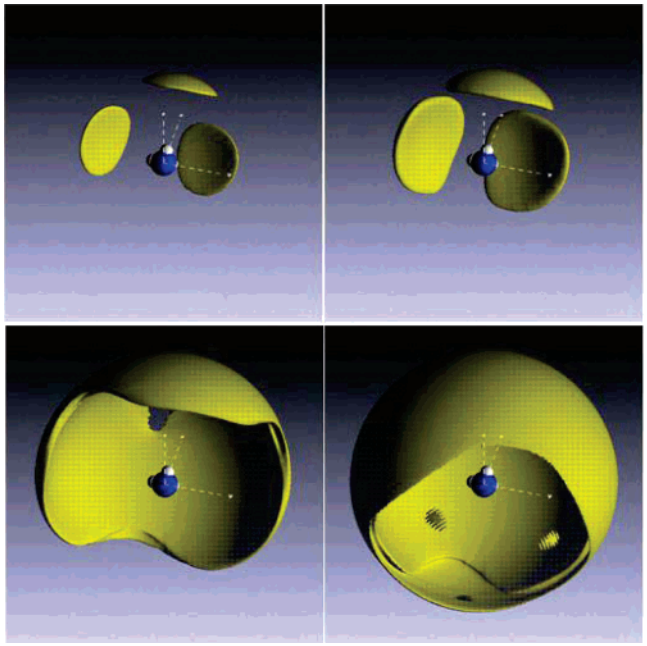

Figure 9. 3D fulleride anion solvation structure as a function of distance to the center of C_{60}^{5-} anions. The yellow region shows the most likely angular positions that a C_{60}^{5-} anion can be found in with respect to a fixed ammonia molecule (Figure 2). This is plotted from 0 to 7.5 Å (top) and 8.8 to 10.5 Å (bottom) to the center of the fulleride anion, which is equivalent to the distances of the two solvation shells. The figure plots the 50% (left) most likely positions and 90% most likely (right).

two or three hydrogen atoms point toward the center of mass. However, the overall dipole moment orientation of the ammonia molecules is the same in the second shell as in the first due to cross-shell H-bonding among the ammonia molecules.

The coordination numbers reveal ∼45 nitrogen atoms, and hence ammonia molecules, in the first solvation shell. Out of these, there are ∼40 H-bonds to the C_{60}. Therefore ∼90% of the ammonias in this shell form H-bonds to the fulleride. At first sight, an average of just less than one H-bond per ammonia to the anion in the first shell may seem small because the anion is relatively highly charged. However, by adopting this orientation the ammonia molecules can then complete H-bonds within and across the solvation shells. Although about half of all the total solvent molecules are involved in the solvation shell, this is why there is no significant change in the average solvent−

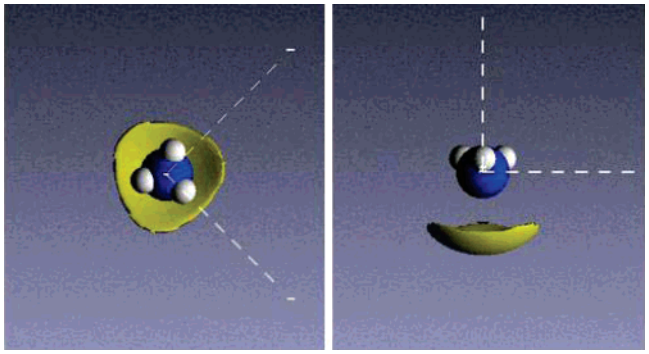

Figure 10. Potassium cation solvation by ammonia. The yellow region shows the most likely angular positions that a potassium cation can be found in with respect to a fixed ammonia molecule. The ammonia molecule directs its nitrogen atom toward the cation.

solvent structure of the fulleride solution from the pure ammonia solvent structure.

The partial $g_{\alpha\beta}(r)$ values show that the average nearest-neighbor C···H and C_{60}···H (C_{60}^{5-} center of mass) distances are 2.60 and 5.80 Å, respectively (i.e., a difference of 3.2 Å). The fulleride cage radius itself is 3.54 Å, suggesting that the ammonia molecules are typically located over the pentagonal and hexagonal rings allowing for a closer approach. There are ~40 H-bonds per fulleride, which gives ~1.25 bonds per carbon ring. The unusually short C···H hydrogen bond lengths of ~2.6 Å are consistent with those observed in solid $(ND_3)_8Na_2C_{60}$ and $(ND_3)_xNaRb_2C_{60}$ (C···D ~ 2.55 to 2.76 Å) in which the ammonia molecules are coordinated to both the fulleride and metal ions.[12]

5.3. Potassium Solvation Structure. The potassium cation solvation can be investigated by examining the $g_{KN}(r)$ and $g_{KH}(r)$, shown in Figure 5, and the spherical harmonic plot, shown in Figure 10. This latter diagram shows the most likely orientational position of a potassium cation with respect to an ammonia molecule. From the coordination numbers shown in Table 2, we find that the cations are solvated by ~6.6 ammonia molecules at an average distance of ~2.9 Å. As one would expect, the cations are solvated with the more electronegative nitrogen atom pointing directly toward them. The value of the K−N distance is almost identical to that found in a neutron diffraction experiment of potassium-ammonia solution,[31] and the effect of the fulleride on the solvation of the potassium cation appears minimal.

The potassium solvation also explains the reduced total number of H-bonds that exist in our solution when compared to pure ammonia. There are on average 6.6 nitrogen atoms solvating the potassium ions, which are not involved in intersolvent H-bonding. There are 5 potassium ions per 250 solvent molecules, and in the pure solvent there are ~2 H-bonds per nitrogen atom. This means that $5 \times 6.6 \times 2 = 66$ fewer H-bonds are expected per 250 ammonias. In pure ammonia, ~2 H-bonds form per nitrogen, giving roughly 500 bonds per 250 ammonia molecules. If we subtract from this the 66 bonds unable to form due to cation solvation, we obtain ~436 (i.e., ~1.74 N−H H-bonds on average per nitrogen. This is consistent with the value obtained from the analysis in section 5.1.

5.4. Anion−Cation Structure. The fulleride is a negatively charged anion, and it is pertinent to examine whether cation−anion pairs will form. For this reason, the partial distribution function for potassium around the center of a C_{60}^{5-} is shown in Figure 11. The statistics for this function are relatively poor, due to the relatively low concentration of the cations (Table 1). However, we see at once that there is a peak due to "inner-sphere" potassium cations closely coordinated to the C_{60}^{5-}. The number of cations in this innersphere is ~1.7 ± 0.7 per fulleride with an average C−K distance of ~3.2 Å. The distances involved are not greater than the respective C_{60}−H and C−H distances, but are similar to those found in K_3C_{60} crystals.[2] Although ion pairs do form, the frequency of them occurring is not high, due to the strength of the respective potassium and fulleride solvation by the ammonia molecules.

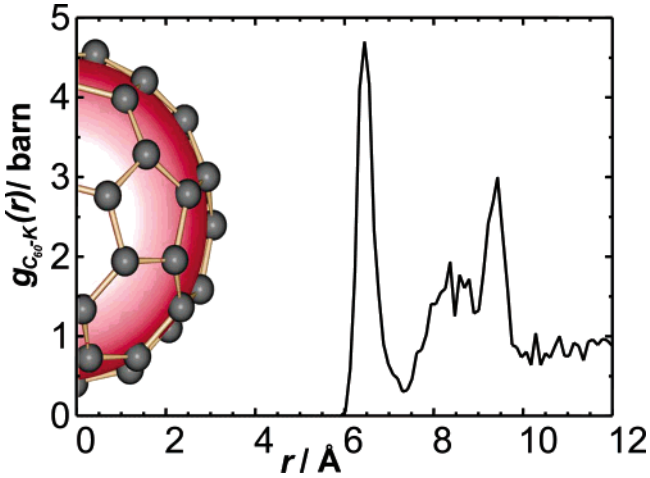

Figure 11. Pair distribution of potassium around the center of a C_{60}^{5-} anion with molecular graphics to guide the eye.

Finally, we comment in passing on fulleride−fulleride correlations. In this context, strong conclusions cannot be drawn directly from our data as the relevant features arise at lower values of Q than those measured here. However, the strength of the solvent ordering, and the resulting structure of the solvation shells around the C_{60} anions, indicate that interfulleride contacts are absent. The solute molecules are therefore dispersed via solvent-separation.

6. Conclusions

We conclude that in $C_{60}K_5(NH_3)_{250}$ solutions the C_{60}^{5-} anions are strongly solvated by a shell of ~45 ammonia molecules, located around 6−7 Å from the center of the fulleride. These molecules direct one of their hydrogen atoms toward the center of the fulleride anion, while retaining axial H-bonding within the shells. This means that the overall solvent structure is similar to that found in bulk ammonia despite the high fulleride concentrations. The potassium ions are typically solvated in the same way as in a metal-ammonia solution of the same metal concentration. The picture built up from these results is a solution in which the cations and anions are tightly solvated. This prevents the recombination of the salt and permits high concentrations of monodispersed fullerides. The results show that these solutions are suitable for studying isolated fulleride anions in solutions where the concentration of fulleride needs to be high, such as in NMR spectroscopy.

Acknowledgment. We thank Daniel Bowron, John Dreyer, John Bones, Chris Goodway, and Rob Done (ISIS Facility) and Peter Edwards (Oxford University) for many useful discussions. We are grateful for financial support from Merck Chemicals Ltd, the UK Engineering and Physical Sciences Research Council (EPSRC), and the ISIS Neutron Scattering Facility.

References and Notes

(1) Kroto, H. W.; Heath, J. R.; O'Brien, S. C.; Smalley; R. E. *Nature* **1985**, *318*, 162.

(2) Andreoni, W. *The Physics of Fullerene-Based and Fullerene-Related Materials*; Kluwer Academic Publishers: Dordrecht, The Netherlands, 2000.

(3) Kadish, K. M.; Ruoff, R. S. *Fullerenes Chemistry Physics and Technology*; Wiley-Interscience: New York, 2000.

(4) Bezmel'nitsyn, V. N.; Eletskiĭ, A. V.; Okun', M. V. *Phys.-Usp.* **1998**, *14* (11), 1091.

(5) Krätschmer, W.; Lowell, D. L.; Fostiropoulos, K.; Huffman, D. R. *Nature* **1990**, *347*, 354.

(6) Buffinger, D. R.; Ziebarth, R. P.; Stenger, V. A.; Recchia, C.; Pennington, C. H. *J. Am. Chem. Soc.* **1993**, *115*, 9267.

(7) Reed, C. A.; Bolskar, R. D. *Chem. Rev.* **2000**, *100*, 1075.

(8) Thompson, J. C. *Electrons in Liquid Ammonia*; Clarendon: Oxford, 1976.

(9) Fullagar, W. K.; Gentle, I. R.; Heath, G. A.; White, J. W. *J. Chem. Soc., Chem. Comm.* **1993**, *6*, 525.

(10) Zhou, O.; Fleming, R. M.; Murphy, D. W.; Rosseinsky, M. J.; Ramirez, A. P.; van Dover, R. B.; Haddon, R. C. *Nature* **1993**, *362*, 433.

(11) Margadonna, S.; Prassides, K. J. *Sol. Stat. Chem.* **2002**, *168*, 639.

(12) Margadonna, S.; Aslanis, E.; Prassides, K. *J. Am. Chem. Soc.* **2002**, *124*, 10146.

(13) Thompson, H.; Wasse, J. C.; Skipper, N. T.; Howard, C. A.; Bowron, D. T.; Soper, A. K. *J. Phys. Condens. Matter* **2004**, *16*, 5639.

(14) Soper, A. K. *Chem. Phys.* **1996**, *202*, 295.

(15) Soper, A. K. *Mol. Phys.* **2001**, *99*, 1503.

(16) Dixit, S.; Crain, J.; Poon, W. C. K.; Finney, J. L.; Soper, A. K. *Nature* **2002**, *416*, 829.

(17) Howard, C. A.; Thompson, H.; Wasse, J. C.; Skipper, N. T. *J. Am. Chem. Soc.* **2004**, *126*, 13229.

(18) Benmore, C.; Soper, A. K. *The SANDALS Manual*; RAL-TR-98-006; Rutherford Appleton Laboratory: Oxfordshire, U.K., 1998.

(19) Wasse, J. C.; Howard, C. A.; Thompson, H.; Skipper, N. T.; Delaplane, R. G.; Wannberg, A. *J. Phys. Chem.* **2004**, *121* (2), 996.

(20) Soper, A. K.; Howells, W. S.; Hannon, A. C. *Atlas-Analysis Time-of-flight Diffraction Data from Liquid and Amorphous Samples*; RAL-TR-89-046; Rutherford Appleton Laboratory: Oxfordshire, U.K., 1989.

(21) Soper, A. K. In *Neutron Scattering Data Analysis*, IOP Conference Series Number 107; Johnson, M. W., Ed.; IOP Publishing: Bristol, 1990; pp 57−67.

(22) Soper, A. K. *Local Structure from Diffraction*; Billinge, S. J. L., Thorpe, M. F., Ed.; Plenum Press: New York, 1998.

(23) Rizzo, R. C.; Jorgensen, W. L. *J. Am. Chem. Soc.* **1999**, *121*, 4827.

(24) Chandrasekhar, J.; Spellmeyer, D.; Jorgensen, W. L. *J. Am. Chem. Soc.* **1984**, *106*, 903.

(25) Åqvist, J. *J. Phys. Chem.* **1990**, *94*, 8021.

(26) Guo, Y. J.; Karasawa, N.; Goddard, W. A. *Nature* **1991**, *351*, 464.

(27) Thompson, H.; Wasse, J. C.; Skipper, N. T.; Hayama, S.; Bowron, D. T.; Soper, A. K. *J. Am. Chem. Soc.* **2003**, *125*, 2572.

(28) Salmon, P. *Proc. R. Soc. London, Ser. A* **1994**, *445*, 351.

(29) Bowron, D. T.; Finney, J. L. *J. Chem. Phys.* **2003**, *118* (18), 8357.

(30) Ricci, M. A.; Nardone, F. P.; Andreani, C.; Soper, A. K. *J. Chem. Phys.* **1995**, *102*, 7650.

(31) Wasse, J. C.; Hayama, S.; Skipper, N. T.; Benmore, C. J.; Soper, A. K. *J. Chem. Phys.* **2000**, *112*, 7147.

(32) Howard, C. A.; Thompson, H.; Wasse, J. C.; Skipper, N. T. *J. Am. Chem. Soc.* **2004**, *126*, 13229.